Quantum Confinement and Host/Guest Chemistry: Probing a New Dimension

Galen D. Stucky, James E. Mac Dougall

Science, New Series, Volume 247, Issue 4943 (Feb. 9, 1990), 669-678.

Your use of the JSTOR database indicates your acceptance of JSTOR's Terms and Conditions of Use. A copy of JSTOR's Terms and Conditions of Use is available at http://www.jstor.org/about/terms.html, by contacting JSTOR at jstor-info@umich.edu, or by calling JSTOR at (888)388-3574, (734)998-9101 or (FAX) (734)998-9113. No part of a JSTOR transmission may be copied, downloaded, stored, further transmitted, transferred, distributed, altered, or otherwise used, in any form or by any means, except: (1) one stored electronic and one paper copy of any article solely for your personal, non-commercial use, or (2) with prior written permission of JSTOR and the publisher of the article or other text.

Each copy of any part of a JSTOR transmission must contain the same copyright notice that appears on the screen or printed page of such transmission.

Science is published by The American Association for the Advancement of Science. Please contact the publisher for further permissions regarding the use of this work. Publisher contact information may be obtained at http://www.jstor.org/journals/aaas.html.

Science
©1990 The American Association for the Advancement of Science

JSTOR and the JSTOR logo are trademarks of JSTOR, and are Registered in the U.S. Patent and Trademark Office. For more information on JSTOR contact jstor-info@umich.edu.

©2001 JSTOR

http://www.jstor.org/
Mon Jun 4 12:15:13 2001

Quantum Confinement and Host/Guest Chemistry: Probing a New Dimension

GALEN D. STUCKY AND JAMES E. MAC DOUGALL

Nanoparticulate metals and semiconductors that have atomic arrangements at the interface of molecular clusters and "infinite" solid-state arrays of atoms have distinctive properties determined by the extent of confinement of highly delocalized valence electrons. At this interface, the total number of atoms and the geometrical disposition of each atom can be used to significantly modify the electronic and photonic response of the medium. In addition to the novel inherent physical properties of the quantum-confined moieties, their "packaging" into nanocomposite bulk materials can be used to define the confinement surface states and environment, intercluster interactions, the quantum-confinement geometry, and the effective charge-carrier density of the bulk. Current approaches for generating nanostructures of conducting materials are briefly reviewed, especially the use of three-dimensional crystalline superlattices as hosts for quantum-confined semiconductor atom arrays (such as quantum wires and dots) with controlled inter–quantum-structure tunneling.

THE EVOLUTION OF ELECTRONIC TRANSPORT MEDIA TOwards the nanosize regime has revolutionized electronic device development in terms of response times and transport efficiency. As one approaches this dimensionality, however, a point is reached where the differentiation between surface and bulk atoms can no longer be ignored in describing either structural or physical behavior, and the number and disposition of even a few atoms with respect to each other becomes critical in understanding the electronic or optical behavior. This is a meeting ground for the chemist and the solid-state physicist. Traditionally, chemists have thought in terms of isolated molecules where the electronic wave function is defined in terms of only a few atoms, while at the other end of the spectrum, physicists have viewed bulk solids as extended periodic arrays of atoms with a nearly continuous distribution of states and bands of energy levels that define the electronic wave function. Science has created the necessary tools and language to model these two extremes but only with the synthesis of nanostructures at this interface is it possible to study and develop a working, predictive science for understanding quantum-confined structures.

In highly polarizable materials such as intrinsic semiconductors, the availability of vacant states can result in extended anharmonic potential surfaces and correspondingly large nonlinear responses. As one might expect, changes associated with quantum confinement, that is, restriction of the electronic wave function to smaller and smaller regions of space, will have profound effects on the nonlinear displacement of charge with optical electromagnetic fields. The ability to generate nanostructure quantum-confined materials atom by atom in the context of recent scientific developments in nonlinear phenomena (*1*) is both an intriguing and potentially rewarding challenge.

As an example, consider electrooptic and optical switching. Because photons travel three orders of magnitude faster than electrons in media, they have obvious advantages for signal transmission (*2*). The combination of electronics and photonics that has been used in optical signal processing and particularly optical switches can be dramatically improved if the slowest member of the chain, that is, the electric signal used to induce refractive index changes necessary for optical switching, is eliminated. Recent theoretical and experimental results indicate a dramatic change in the linear and nonlinear optical (NLO) response as a function of decreasing the size of semiconductor atomic clusters (*3, 4*) to the point of quantum confinement. The use of the NLO response of these near "molecular" clusters provides a means to optically switch with photons alone at correspondingly faster response times.

In order to demonstrate this, consider an idealized experimental device based on the old idea first described by Fabry-Perot in 1897 (Fig. 1). Transmittance of light through the resonant cavity is permitted only if the cavity dimensions are a half integral of the wavelength. The resonance path length d can be changed by varying the wavelength of light, the length of the resonant cavity, or the refractive index of the media within the cavity. In the classical experiment the refractive index is varied only by changing the optical medium of the cavity. With NLO nanosize (quantum-confined) semiconductors as the optical medium, the refractive index and the

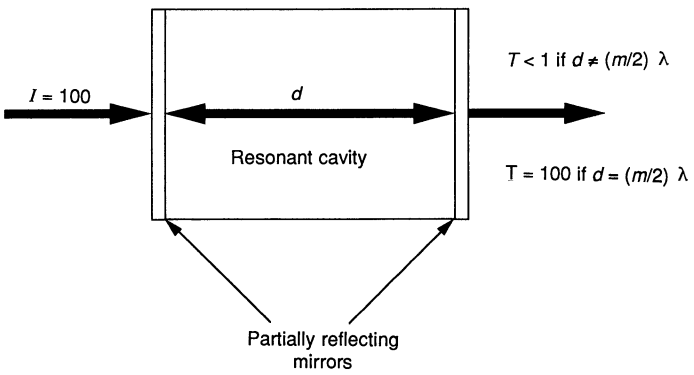

Fig. 1. Fabry-Perot resonant cavity.

The authors are in the Department of Chemistry of the University of California, Santa Barbara, CA 93106.

absorption edge vary with the light intensity so that one can create an optical transistor (*5*) (Fig. 2A).

In Fig. 2A the currently realistic point of view is taken that our efforts at quantum confinement have resulted in the generation of narrow valence and conducting bands. As the intensity of the excitation light is increased, the absorption edge (λ_1) at first changes slightly with filling of the lowest energy states (*6*). This in itself is a nonlinear process with a corresponding change in the refractive indices. Upon saturation of the transition, when the rate of filling is equal to the rate of depletion of the lowest energy excited state band, any additional photons absorbed must have higher energy (λ_2) in order to promote electrons into the next available state. Photons with lower energy are then transmitted so that the intensity selectivity in Fig. 2A is achieved. In short, when saturation conditions as a function of the laser intensity are obtained, the interferometer becomes transparent for the laser light (λ_1) and optical switching takes place.

Obviously, the effectiveness of this experiment will depend on how well the resonance cavity can be defined. In reality the "device" would consist of a collection of resonance cavities, the quantum-confined particles, which should all have identical dimensions, absorption, and optical transmission properties. The optical matrix that supports them must maintain their individual structural and electronic integrity with well-defined potential barriers between clusters, ideally creating a three-dimensional (3-D) quantum superlattice.

Considerable effort has gone into the design and study of molecular clusters. In this article we focus on the strategy of using a 3-D crystalline surface to selectively assemble clusters of a given topography and size in a periodic lattice. This is preceded by a brief summary of the methods currently being used to generate the molecular clusters themselves.

Quantum Structures and Atom Assemblies

The basic ideas of quantum confinement or quantum wells were introduced in the early 1970s (*7*). In these nanostructures, the dimensions of the wave function of the electron-hole pair (exciton) in the lowest excited state of the nanocluster are comparable to the physical size of the particle. This quantum confinement of the exciton means that the continuum band of energies becomes more molecular in character, with narrow ranges of energy and line structure in the optical spectra, as illustrated in Fig. 2B (*8*). For the chemist, less delocalization means less energy stabilization; a reflection of this is that the absorption band for direct transitions of nanosized semiconductor clusters is shifted to higher energies than in the extended bulk parent materials. As noted above, "photocharging" of the semiconductor particle, that is, photoinducing high electron concentrations into a narrow conduction band with a small effective density of states, also changes the band gap and the resulting absorption edge. In addition to NLO applications, the phenomena can be used to carry out electron-transfer processes that are otherwise inaccessible to the bulk semiconductor (*6*).

Most importantly for NLO is that strong nonlinear responses are observed near exciton resonances, a feature not available in comparable materials with no quantum confinement (*15, 16*). In quantum structures the number of states that are available in the relatively small energy band can be very limited, so that adding or removing only a few carriers can substantially change the absorption edge and thus the optical coefficients (such as the index of refraction). Conversely, perturbation of the quantum cluster by light can modify the optical coefficients and the absorption edge. Small changes in the dielectric properties of the confining structure or the surface states of that cluster also can introduce large changes in optical properties. Quantum confinement can therefore be used to change the position and nature of the resonance absorption transitions, as well as to make the NLO response particularly susceptible to modification by optical and low-frequency electric fields. An additional and equally important property of quantum-confined materials is that ultrafast response times become accessible because of the increased importance of surface states (*10*).

The quantum-structure size that is desirable for optimum NLO response depends on the exciton diameter, the effective separation of hole and electron in the first excited state of the semiconductor. For large band gap semiconductors such as zinc sulfide (*Z*nS, E_g = 3.6 eV) or cadmium sulfide (CdS, E_g = 2.58 eV), quantum confinement will not take place until the particle size is $\lesssim$15 Å or $\approx$35 Å, respectively, although for the small band gap indium antimonide (InSb, E_g = 0.23 eV) the exciton will be delocalized over $\approx 10^6$ atoms with a diameter of $\approx$1400 Å. These numbers are "particle-in-the-box" estimates for quantum boxes or wells, and different considerations apply to quantum wires or sheets.

Experimentally, the architecture of quantum confinement can be achieved in a variety of ways with very different anticipated electrooptic and electronic consequences. An important goal of all approaches is that the synthesis results in monosize configurations (same number of atoms in the confinement dimensions) with a single geometrical arrangement of atoms. For confinement within a single dimension, the Langmuir-Blodgett technique allows one to sequentially deposit a single layer of semiconducting particles within an insulating lattice and then generate a film from multiple layers. In this way, monoatomic layers of CdS, each with a thickness of approximately 3 Å, can be generated by treating Langmuir-Blodgett layers of cadmium arachidate with hydrogen sulfide (H_2S) (*11*). The onset of absorption of a layer is blue-shifted by 0.38 eV with respect to bulk CdS and insensitive to the number of Langmuir-Blodgett layers deposited (up to seven), which suggests no strong electronic interactions between successive layers. For optical applications a

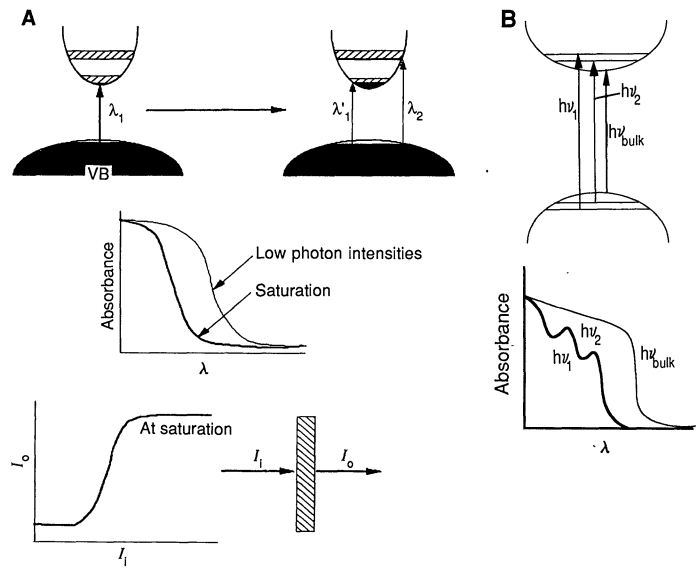

Fig. 2. (**A**) Quantum-confinement effects on optical absorption. As the photon intensity *I* is increased, a small blue shift ($\lambda_1 \rightarrow \lambda_1'$) is first observed that is due to photoinduced changes in the electron concentrations in the valence (VB) and conduction bands (*6*). At saturation, only photons with wavelength λ_2 are absorbed. (**B**) The quantum-confinement effect results in a band edge shift (dark line on left) to higher energies from $h\nu_{bulk}$ and line structure in the optical absorption spectrum. The discrete energy levels $h\nu_1$, $h\nu_2$, and so forth arise as a result of limiting electron-hole delocalization by particle-size dimensions.

limitation of this approach is the difficulty in obtaining films with an optical thickness on the order of a micrometer or more.

Recently, chemists have approached the problem of controlling 3-D constrained cluster geometries by a molecular approach (*12*). The procedure is to use solution chemistry with arrested precipitation to form the semiconductor cluster followed by kinetic capping of these clusters with organic groups (*13–16*). Quantum confinement is then in all three dimensions, and the structures are referred to as quantum dots or boxes. Nature also creates similar quantum-dot clusters of CdS in an elegant way by using short chelating peptides in yeast as part of the biochemical mechanism of entrapping heavy metal atoms such as Cd (*17*). At the time of their characterization, these clusters were found to be more monodisperse than those which had been prepared chemically.

The physicist's and engineer's strategy has been based on molecular beam (MBE) and atomic layer epitaxy (ALE) (*18*), which makes possible the fabrication of ultrathin (monolayer) semiconductor epitaxial layers. Carrier confinement is then achieved by sandwiching the semiconductor layer between two semiconductor epitaxial layers with wider band gaps or by introducing lateral barrier walls to form quantum boxes (*19*). Quantum wires, in which carriers and electronic wave functions have one degree of freedom along an axis, can be formed in the MBE approach by corrugation of quantum layers or by lateral structuring (*20*). A promising new development is the use of the scanning tunnel microscope (STM) as a lithographic tool to create the barriers on the 10 to 1000 Å scale (*21*).

The actual real world results that have been reported to date for quantum dots are in consensus with the observation of a blue (higher energy) shift in the optical absorption spectrum with decreasing particle size. However, even in the best samples of quantum structures, there is a distribution of sizes and consequently a smearing or inhomogeneous broadening of the optical spectrum so that the sharp optical spectrum and narrow energy bands are lost (*22*). These results are a reflection of the extremely high resolution and synthetic quality that is required to generate a precisely defined individual quantum clusters and the super quantum lattices. In the growth of quantum clusters by arrested precipitation from solution, the clusters are obtained by quenching a kinetic process in which the systems' drive towards thermodynamic equilibrium is interrupted. These methods are capable of the reproduction of quantum-particle diameters on the order of 20 to 100 Å to within 3 to 5% by making use of lattice matching or by using a host nucleation site such as inverse micelles in arrested precipitation (*15*). If we assume an atomic diameter of 2 Å, this corresponds to 4 to 5 atoms out of every 100 atoms. In order to achieve the necessary resolution to see the exciton bands, either more carefully controlled synthetic conditions or another approach is needed. Alivisatos and co-workers (*22*) have estimated that a 1% variation in cluster diameter (roughly 1 out of every 100 atoms) must be achieved to observe discrete excitonic features in the absorption spectra. At these levels of accuracy in building quantum structures, phonon-electron coupling can be equally important in determining the sharpness of the quantum-structure exciton transitions.

The bulk NLO response depends on the number of polarizable electrons per unit volume so that a high-density collection of quantum nanoclusters is required, both for achieving a basic understanding of the quantum-structure phenomena and for device development. In designing such devices, one, by necessity, must consider not only the atomic construction of the individual quantum wires, boxes, sheets, and rings, but also the assembly of these into a macroscopic unit. Glasses (*23*) and polymers (*4, 24*) have the advantage of being readily made into thin films for device application, but the disadvantage of having particle size distributions, which in present commercial samples typically vary by more than 10% (*25*). The consequence is that the exciton resonances are broadly distributed in energy so that wavelength-selective NLO phenomena are difficult to achieve.

Table 1. T_d Corner-shared molecular sieve compositions.

Type	Groups		Charge	Material
IV-IV	SiO_2	SiO_2	0	Silicalite
V-III	PO_2^+	AlO_2^-	0	ALPO
V-IV-III	$(PO_2^+)_{1-\delta}$	$(SiO_2)_\delta AlO_2^-$	$-\delta$	SAPO
IV-III	SiO_2	AlO_2^-	-1	Zeolite
V-II	PO_2^+	ZnO_2^{2-}	1	Zinc phosphate
III-III	BO_2^-	BO_2^-	-2	Boralite
V-II	SiO_2	BeO_2^{2-}	-2	Beryllium silicate (helvite)

In summary, the most challenging problems in the development of quantum-confinement structures have been (i) to reproducibly obtain uniform monosize clusters so that the quantization is accompanied by the concentration of bulk oscillator strength into single spectral lines and (ii) to package these quantum structures in a defined and functionally useful way while maintaining the quantum-well electronic and atomic structure. These two problems have not yet been simultaneously dealt with successfully in any medium.

Inclusion Chemistry and Quantum Structure

In fact, the packaging requirement can be used to good advantage in controlling optical and electronic properties, particularly if materials can be synthesized by producing periodic arrays of these quantum structures, that is, quantum superlattices. The periodicity of these arrays will result in a new mechanism to control band structure, and therefore the photonic and electronic properties. In addition, deviations from periodicity might be selectively introduced which can be expected to both give insight to the effects of disorder, defects, and order-disorder transitions as well as present an opportunity to tune or modify device response.

One way to achieve this is by the self-assembly of quantum-confined clusters or wires in a crystalline host framework. The self-assembly is accomplished by "ship in the bottle" chemistry in which molecules and atoms are reacted within molecules and atoms are reacted within the angstrom-sized channels of a molecular sieve or zeolite host (*26, 27*). It is not like arrested precipitation, since the reactions can go to their thermodynamic completion within the constraints of the 3-D surfaces that define the "reaction chamber" topology. The inclusion chemistry that is used allows selective access one atom or molecule at a time by ion exchange or gaseous diffusion to the cages or channels in which the self-assembly is carried out.

The molecular sieve structures permit one to vary the cluster concentration, intercluster geometry, nature of the quantum well barrier, and the defect chemistry in a controlled manner over the periodicity defined by the host molecular sieve lattice. The framework charge of the open molecular sieve frameworks can be controlled by the types and relative amounts of different metal atoms used in a given host framework (Table 1). For example, pure silicate molecular sieves are hydrophobic, selectively adsorbing aromatic hydrocarbons from water, while the more highly charged frameworks make excellent water traps.

The cages and channels that make up molecular sieves have diameters of up to 13 Å such as those found in zeolite Y (*28*) and ALPO-5 (*29*). The 8 to 13 Å size constraints limit the cross section of individual clusters, although with the appropriate host geometry

(Fig. 3) quantum wires of indefinite length that are one-dimensional or form a 2-D or 3-D grid network are possible. The quantum confinement is not however determined solely by the cross-sectional dimensions of the host channels, since the barriers between the quantum dots are one or two insulating atomic layers thick. This means that resonant and indirect tunneling is possible by phonon-assisted mechanisms through the overlap of wave functions of adjacent clusters (*30*).

Depending on the thermodynamics of the self-assembly and the host/guest interactions, the small clusters might also be used as atoms are in the arrested precipitation approach, that is, a collection of small clusters are used instead of atoms to build the quantum-confined structure. Such structures can be made by controlling the concentration of atoms during the self-assembly. This feature allows one to characterize quantum-lattice effects, systematically starting from the isolated molecular cluster to an arbitrarily large collection of clusters connected by resonance or nonresonance tunneling through the mono- or dilayer insulator walls.

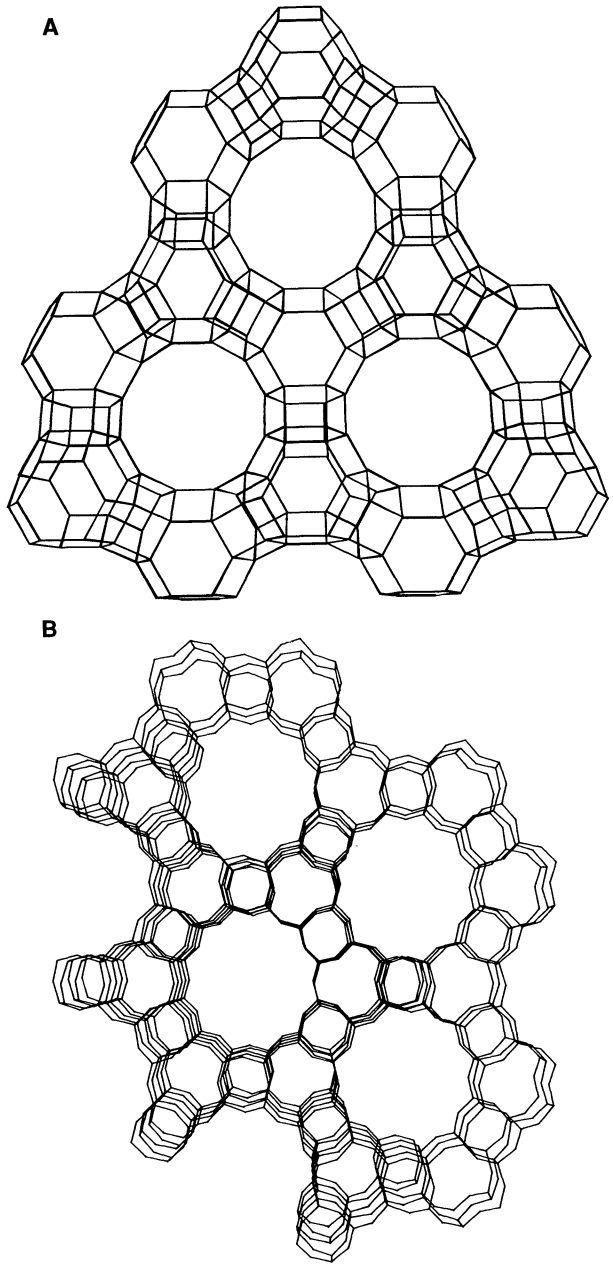

Fig. 3. (**A**) View looking into the 12-ring openings of three supercages of zeolite Y (see Fig. 4B). Oxygen atoms vertices are not included. (**B**) View looking into 12-ring channels (including oxygen atom sites) of ALPO-5.

Table 2. Comparison of selenium band gaps (*36*).

Se sample	Band gap (eV)	Basic unit
t-Se	1.98	Helical chain
α-Se	2.53	Se_8 ring
Se-mordenite	2.25	
Se-ALPO-5	2.4	
Se-A	2.85	
Se-X	2.3	
Se-Y	2.2	

The two major limitations of these materials for NLO applications are the limited cluster sizes and the difficulty in obtaining large, optical quality crystals, with the largest currently available being on the order of 1 to 3 mm and more commonly 0.1 to 0.8 mm. They do provide an important opportunity to study intercluster interactions for charge carrier units in a periodic host so that it is possible to accurately characterize interatomic separations, the details of cluster topography and orientation, and insulator charge effects as a function of optical response. In addition, their chemical composition is the same as that of glasses, so that the chemistry and physics that can be studied in detail by the incorporation of quantum-confined clusters into the crystalline host is particularly useful in the design of devices based on glass hosts. An additional note of promise is that Bein and co-workers have recently successfully been able to synthesize zeolite membranes (*31*) that consist of zeolites imbedded in a glassy matrix. Since the glasses can be made with the same chemical composition and refractive indices as the zeolite host, thin-film optical devices derived from these "chemical sensors" appear to be feasible.

Elemental Semiconductor Superlattices: Se and Te Quantum Confinement and Quantum Wires

Elemental semiconductor confinement represents an almost ideal case to study, since stoichiometry is not a concern during the synthesis. By using the molecular sieve as a host, one can study intercluster interactions either by controlling the guest concentration within the host, or by using different host topographics. The first attempts to synthesize nanocomposites of semiconductor-based clusters in zeolites were carried out more than 10 years ago by Bogomolov (*32*), who also was extensively concerned with the use of zeolite hosts as a means of self-assembling superconducting quantum wires (*23*).

When Se and Te are absorbed into the pore structure of molecular sieves, dramatic differences in the band gap and optical absorption spectra are observed in these materials from the bulk forms (Table 2). The thermodynamically favored form of Se at room temperature and pressure is trigonal Se (t-Se), which consists of helical chains with three Se atoms per repeat unit (*34*). Selenium has several other bulk allotropes that consist of six-, possibly seven-, and eight-membered rings (*35*). Different allotropes can be generated selectively within the molecular sieve framework depending upon the internal 3-D topography. In zeolite A, the optical spectra suggest that rings are formed similar to the monoclinic bulk form (Se_8) (*36, 37*), and Te_8 rings have been observed by Raman spectroscopy in the α cages of zeolite A and in the supercages of zeolite Y (*38*). In the large-cage systems the cluster selectivity begins to break down, as demonstrated by solid-state ^{77}Se magic angle spinning nuclear magnetic resonance (MAS-NMR) spectra, which suggests that

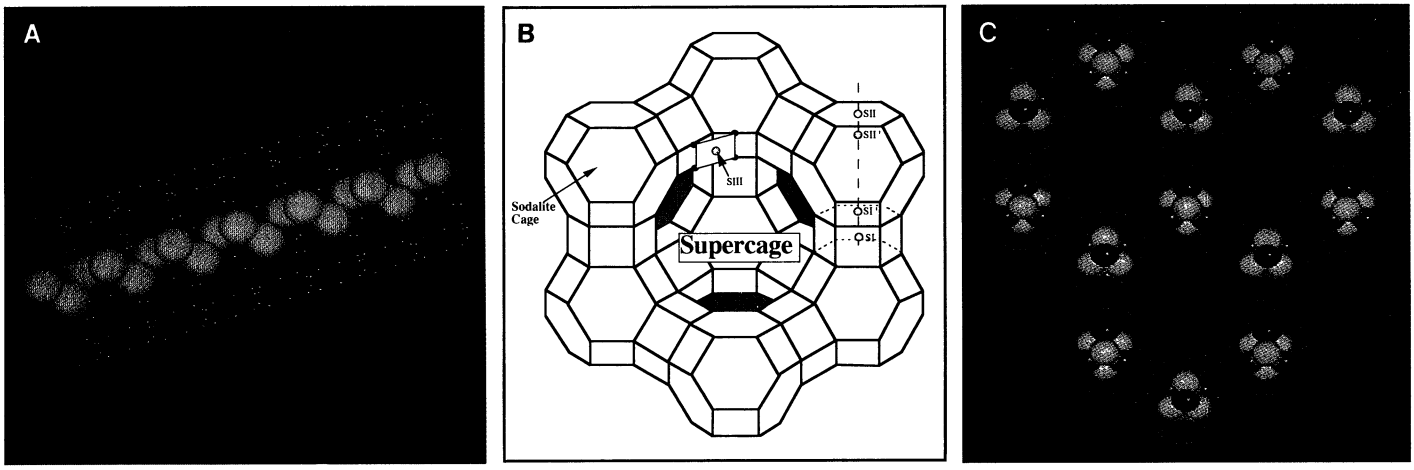

Fig. 4. (**A**) t-Se helical chain (in yellow) in a hexagonal 12-ring channel of ALPO-5. (**B**) Zeolite Y supercage structure, showing selected cation sites. Verticies represent "T" atoms; oxygen atoms have been excluded for clarity, except for the SIII site. (**C**) $(CdS)_4$ clusters in the sodalite cages of zeolite Y. Cadmium and sulfur atoms are orange and yellow, respectively.

several different Se allotropes exist in zeolite Y (*39*).

Selenium loaded in channel systems like ALPO-5 and mordenite appears from optical, ^{77}Se MAS-NMR spectra, and extended absorption x-ray fine structure spectroscopy (EXAFS) (*36, 39, 40*) to exist only in a helical chain conformation similar to that in the trigonal allotrope. Lack of spinning sidebands in the NMR spectra also imply that interchain interactions are minimized and that the Se atoms are in a more nearly spherical environment, as would be the case for an isolated chain that is free to rotate.

A computer-stimulated picture (*41*) of an Se helical chain in the 12-ring (*42*) channels of ALPO-5 based on the above experimental data is shown in Fig. 4A. Packing considerations suggest only one Se helix per channel. If the Se atoms are packed against the walls, the closest interchain approach would be 5.2 Å, which is considerably greater than for bulk t-Se (3.44 Å), where the interchain distance is less than the van der Waals distance (3.8 Å). The observed band gap, 2.4 eV, for Se in ALPO-5 is substantially greater than that of bulk t-Se (1.98 eV) and less than that of Se-A (2.85 eV) or α-Se (2.53 eV), which contain Se_8 rings, as one would expect for isolated quantum-wire helices. The molecular sieve VPI-5 (*43*) is an aluminum phosphate that is similar in structure to ALPO-5, but with larger 1-D 18-ring channels that are 13 Å in diameter. Packing considerations show that two- and perhaps three-strand wires within these channels are feasible. These systems are excellent models for extended quantum-wire confinement in a periodic lattice.

Binary Semiconductors Confinement: Cluster Topography and Quantum Lattices

Host/guest chemistry can also be applied to more complicated and inherently more interesting systems than elemental semiconductors. The inclusion chemistry of I-VII (*44, 45*), II-VI (*46–50*), and III-V (*51*) semiconductors has been investigated concentrating on the structural, optical, and photochemical (*52, 53*) aspects of the clusters.

In the following discussion on binary semiconductor systems, two roles of the superlattice host are emphasized: (i) to define the quantum-confinement geometry, and perhaps more importantly, (ii) to provide the 3-D periodicity to form a "supra-molecular" composition and the overall quantum lattice. Some examples of the use of selective siting and the use of host internal-surface topology to define cluster geometry follow.

Control of Cluster Topography

Zeolite Y, a high-dielectric aluminosilicate host, has two types of cages available for cluster formation, the smaller 8 Å sodalite units and the larger 13 Å α supercages (Fig. 4B). For the purposes of this discussion there are five sites (I, I′, II, II′, III) available for cation siting within the sodalite and supercages. II-VI and I-VII quantum-confined clusters can be synthesized by well-understood ion-exchange methods, followed in the II-VI case by treatment with H_2S or H_2Se. It is important to note that the ion-exchange process can yield very different siting of cations depending on temperature, *p*H, solvent versus melt ion inclusion, other extra-framework ions, calcination, and loading levels. This process must be systematically controlled along with the conditions for treatment with H_2S or H_2Se to obtain materials that can be consistently reproduced and that contain monosize clusters.

For the synthesis of CdS in zeolite Y, careful control of the above ion-exchange parameters permits selective siting of Cd^{2+} at I′ (*54*), which is within the sodalite cage. The zeolite is then treated with H_2S to form the CdS superlattice. At a low loading level of CdS in zeolite Y, isolated CdS molecular units are formed with an absorption peak around 290 nm and no emission even at 4.2 K. At higher

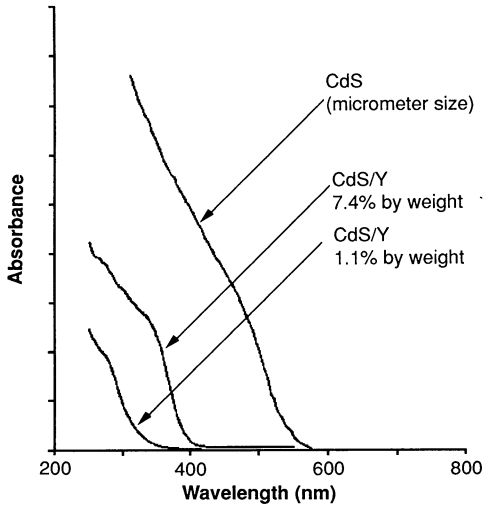

Fig. 5. Absorption spectra as a function of loading level in zeolite Y (*49*).

loadings, x-ray single-crystal (*55*) and powder diffraction, EXAFS, and optical absorption data show that eight-atom $(CdX)_4$ (X = S or O) clusters can be precisely located within the sodalite cages (*46–60*) (Fig. 4C). The discrete clusters within the small sodalite units of the CdS zeolite Y structure begin to interconnect electronically by quantum tunneling as the loading density within the zeolite rises. As is evident in Fig. 4C, the Cd atoms point toward each other through the double 6-rings linking the sodalite units with a Cd-Cd distance of 6.2 Å. As this 3-D interconnection proceeds, the corresponding changes in optical properties (Fig. 5) indicate a progression toward a semiconductor supercluster with behavior intermediate between that of the discrete clusters and bulk semiconductor. The transition from clusters to aggregates upon increasing CdS loading is not continuous but rather abrupt, as judged from optical absorption and emission spectra. This suggests that the aggregation of the individual clusters inside the zeolite may be a percolative process.

When fully loaded, the quantum superlattice shows an exciton shoulder near 340 nm and emits at low temperature. Neither heating nor increasing CdS concentrations can further shift this exciton shoulder to the red. In contrast, when CdS is on the exterior surface of the zeolite crystallite, a continuous red shift of the absorption threshold toward the bulk value is observed, paralleling the behavior of CdS colloids.

The window and cage size of the sodalite unit selectively determines the sodalite cage content. The anionic radii of Se (1.98 Å) and Te (2.21 Å) are sufficiently greater than that of S (1.84 Å) for the formation of the $(CdX)_4$ unit (X = Se or Te) within the sodalite cage to no longer be thermodynamically unique or feasible (*56*). After Cd^{2+} ion exchange and treatment with H_2Se, 70% of the Cd ions are found at site I′ within the sodalite cage and 30% are at site III within the large supercage in 12-ring windows where they are coordinated to Se atoms within the supercage. Large-cation II-VI units such as PbS can also be synthesized within the large supercage of zeolite Y (*46, 52, 55*). The PbS molecule is inherently quite stable, and detailed analysis of synchrotron x-ray absorption data of the Pb LIII-edge shows that monomolecular PbS_2^{2-} species are anchored to the zeolite supercage framework, but to date no polynuclear clusters have been identified.

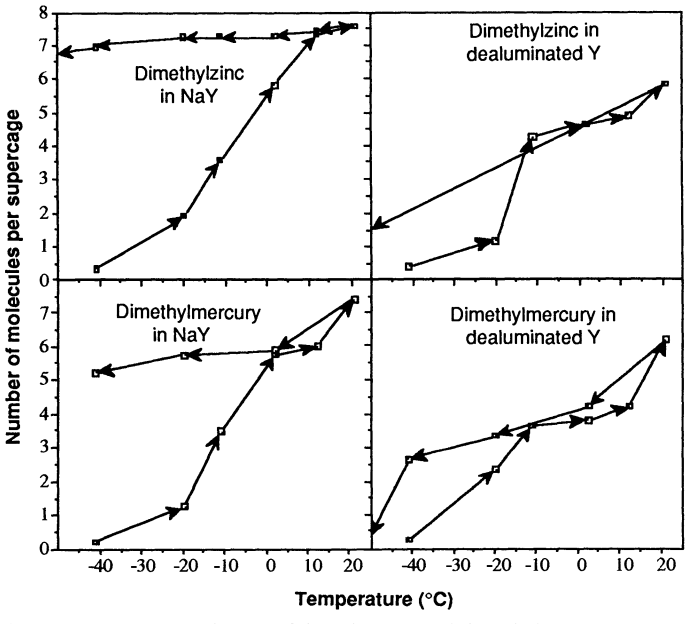

Fig. 6. Adsorption isotherms of dimethylzinc and dimethylmercury in NaY and dealuminated Y; Si:Al ~700:1. Arrows indicate the order in which the data was obtained. Full vacuum was applied to the samples for the last point when it is on the left axis.

Telluride siting has been worked out in detail by Olson and coworkers (*57*) from single-crystal x-ray diffraction studies. Zeolite X has the same framework geometry as does zeolite Y, but with an Al:Si ratio of 1.25. A different synthetic approach was used, namely high-temperature diffusion of Te into the cages of a dehydrated Na zeolite X, followed by treatment with hydrogen. In a lightly loaded zeolite (4.5% by weight of Te) the Te atoms are distributed between the supercage and the center of the sodalite cage in a 3:1 ratio. In the sodalite cages, the cluster unit is Na_4Te (Na-Te distance of 2.59 Å), which is analogous to the Ag_4Br, Cd_4S, or Ga_4P units that have been synthesized in the sodalite–structural-type crystallographic phases (see below).

The Te siting in the supercage is particularly interesting as it defines the preferred potential surface siting within the supercage for Te ions. By using the crystallographic coordinates of Olson, one can address the question of the feasibility of forming a large Te cluster within the supercage of a zeolite X structure at full loading. The formal oxidation state of Te in such a cluster and the extra framework cation charges could be adjusted to balance the cage charge.

The full-occupancy model of the $Na_{10}Te_{12}$ supercage cluster derived from the single-crystal x-ray diffraction coordinates has Te-Te distances of 2.73 Å and 3.36 Å (compare with 2.84 to 3.00 Å in elemental Te and 2.68 to 3.10 Å for Te_6^{4+}) (*58*). Since the supercage Te sites are not fully occupied at the loading levels used by Olson, such a 22-atom cluster is yet to be synthesized. However, the data give a good indication of the size and type of clusters that might be self-assembled within the zeolite Y supercage structural type from known potential well siting.

Another method for controlling the individual cluster topology is to use organometallic precursors that are sterically restricted to large channels or cages with either a metal organic chemical vapor deposition (MOCVD) (*51*) or photochemical dissociation and reaction (*59*) approach to accomplish cluster synthesis. For example, in zeolite Y the organometallic precursor molecules are too large to enter the "β" cages, and cluster formation can selectively take place in the supercages. Either of these methods requires that one carefully consider the role of the host cage or channel walls and how they will ultimately define the quantum-confined structure.

In general, molecular sieve host frameworks can be regarded as 3-D accessible surfaces consisting of monolayer TO_2 (T is a framework atom, such as Si, Al, or P) units. The 3-D internal surface of the zeolite can be used to both delineate the ultimate quantum-confinement geometry, such as clusters or wires, and as a reaction framework upon which to build the cluster. The 3-D host surface can be functionalized by attaching molecular units such as phosphates (*60*) or silicates (*61*) and the framework charge can be varied by atom substitution (Table 1).

One example of the importance of this in zeolite cluster formation is illustrated in Fig. 6, which shows the adsorption isotherms of dimethylzinc and dimethylmercury in zeolite Y with Si:Al ratios of 3.2 and 700 from vacuum (10^{-5} torr) at −45°C to the vapor pressure of the organometallic at 20°C (*62*). The greater reactivity of dimethylzinc with the molecular sieve framework is shown in the nearly complete irreversibility of its adsorption into NaY (Fig. 6, upper left). Dimethylmercury in NaY (Fig. 6, lower left) shows a two-step adsorption curve indicating that above about six molecules per supercage, which may correspond to a monolayer of surface coverage, there is fully reversible adsorption. In dealuminated Y, which has essentially zero framework charge, both dimethylzinc and dimethylmercury adsorb reversibly. Opportunities clearly exist to use the electric (charge carrier and insulator) and chemical-bonding properties of the molecular sieve internal surface to control both the

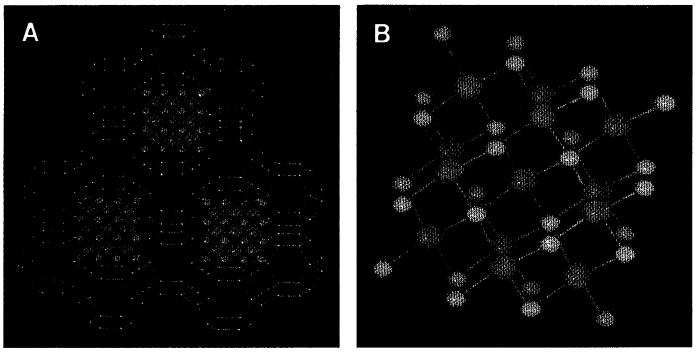

Fig. 7. (**A**) $Ga_{28}P_{13}$ clusters in the supercages of zeolite Y, as viewed through the 12-ring windows into the supercages. Gallium and phosphorus atoms are yellow and green, respectively. (**B**) $Ga_{28}P_{13}$ cluster model showing three coordination spheres around phosphorus, based on EXAFS and ^{31}P MAS-NMR study of GaP in zeolite Y.

self-assembly chemistry and the ultimate quantum-confinement geometry.

The III-V synthesis of "GaP" has been carried out by the MOCVD reaction of trimethylgallium and phosphine in the cages of zeolite Y. The supercage point-group symmetry is $\bar{4}3m$, the same as bulk GaP, which is expected to help in obtaining periodic and local ordering. The synthesis cannot be readily achieved by ion exchange of the group III metal cation into the zeolite because of *p*H restrictions. The use of organometallic precursor chemistry can result in the formation of clusters as large as the 26 to 28 atoms $[(GaP)_{13-14}]$ in the supercages (Fig. 7), (*51*) while restricting Ga atom migration into the smaller sodalite cages. The course of the reaction has been carefully monitored by ^{31}P MAS NMR (*51*) and optical spectroscopy as a function of reaction temperature and loading for both NaY and the acid zeolite HY. For example, near the optimum reaction temperature in NaY, a 25°C change in PH_3 reaction temperature dramatically changes both the optical properties and the structural character of the end material. In HY, trimethylgallium molecules are first anchored at room temperature by the elimination of methane to give $[(CH_3)_2Ga]OZ$, where OZ refers to the zeolite framework O atoms.

The GaP cluster structure in zeolite Y has been studied by EXAFS and synchrotron x-ray diffraction. A model consistent with the results of these studies and ^{31}P MAS NMR is shown in Fig. 7. The figure shows the largest cluster formed, and it should be emphasized that full occupancy of each atomic site in every supercage has not been demonstrated. GaP has both an indirect and direct band gap with E_g = 466 nm direct, 546 nm indirect. The absorption spectrum in Fig. 8 shows pronounced peaks at 350 nm or less that are blue-shifted relative to bulk GaP. The samples absorb to the red of bulk GaP, which may result from the transformation of an indirect to a direct band gap in the quantum-confined material.

The organic-capped molecular clusters of "CdS" described above (*15*) actually have Cd:S ratios that are significantly different than 1:1. A ten-Cd atom cluster that has been structurally characterized has the empirical formula $Cd_{10}S_4(SC_6H_5)_{16}$ with a Cd:S (sulfide) ratio of 10:4, the rest of the metal atom sites being occupied by "surface state" thiol S atoms (*13*). The atomic composition of the GaP cluster in Fig. 7B is $Ga_{28}P_{13}$, with the Ga atoms on the surface of the cluster completing their first coordination sphere by bonding to the framework O atoms of the host.

An important new approach to synthesizing transition metal oxide quantum-confined structures in molecular sieve hosts has been recently reported by Ozin and Ozkar (*59*). In this case the precursor organometallic molecule is a binary metal carbonyl such as $W(CO)_6$. Instead of a MOCVD thermal epitaxy approach to the quantum-confined cluster, tungsten oxide (WO_3, E_g = 2.7 eV) is synthesized at room temperature or below by photochemical dissociation in the presence of O_2. This method greatly reduces the possibility of C and H atom impurities that must be dealt with in the MOCVD synthesis.

At loadings of less than one WO_3 unit per supercage, the absorption edge is blue-shifted from the bulk WO_3 band gap edge to 3.5 eV. When the concentration is more than one WO_3 unit per supercage, there is an abrupt shift of the absorption edge to a limiting value of 3.3 eV, which is maintained to the highest loading composition of roughly four WO_3 units per supercage. Fourier-transform infrared spectroscopy (FTIR), MAS-NMR, x-ray photoelectron spectroscopy, and preliminary x-ray diffraction data suggest the formation of $(WO_3)_4$ cubane-like structures within the supercages. Ozin and Ozkar have been able to make use of the host framework chemistry to anchor the clusters by using the acid HY zeolite to generate hydrogen bonding between the framework and the WO_3 oxygen atoms. For the full-volume filling of the supercages, the quantum-confined WO_3 clusters are organized into a quantum superlattice with long-range coupling through tunneling between cage clusters. The known electrochromic, solid-state ion insertion, and electronic-ionic transport of bulk WO_3 make this a fascinating quantum-confinement system to study.

Control of Intercluster Properties: The Quantum Superlattice

The high stability of quantum-confined clusters inside the sodalite units in zeolite Y is due to the coordination of Cd atoms with the framework O atoms of the double 6-ring windows. Quantum well tunneling through the aluminosilicate cage wall is suggested to be responsible for the interaction between clusters (*46, 48, 49*). If this is correct, one would expect to be able to vary the absorption edge by changing either the periodicity, that is the spacing between clusters, or the framework composition. Zeolite A can be structurally derived using the same sodalite cage as in zeolite Y (Fig. 9A). The geometrical difference is that in zeolite Y the sodalite cages are

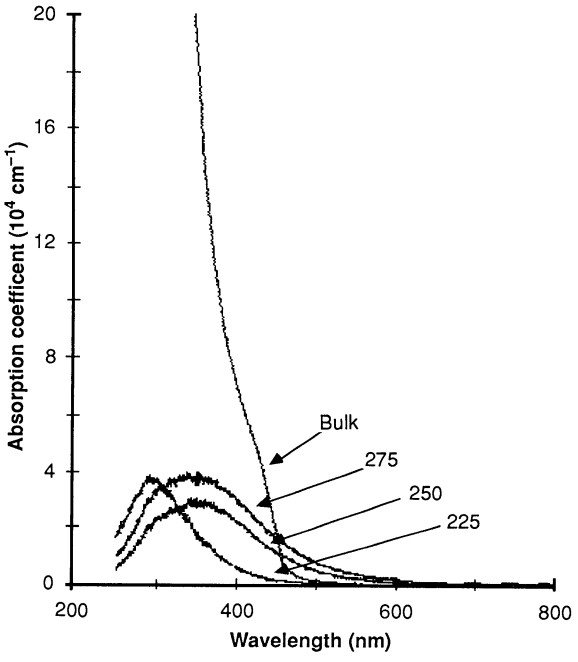

Fig. 8. UV-visible spectra of bulk GaP, and GaP included in zeolite NaY, treated at 225°, 250°, and 275°C in PH_3.

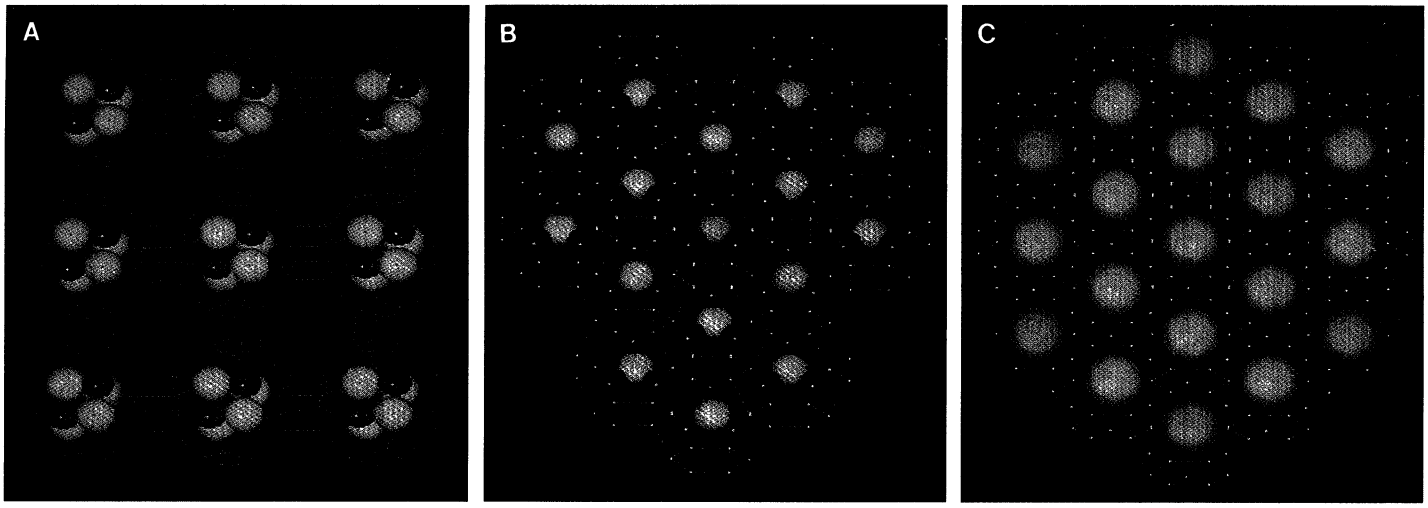

Fig. 9. (**A**) $(CdS)_4$ clusters in the α cages of zeolite A. Cadmium and sulfur atoms are orange and yellow, respectively. (**B**) Zn_4S clusters in the sodalite-type host, boralite. Zinc and sulfur atoms are orange and yellow, respectively. (**C**) Expanded semiconductor lattice of M_4X molecular clusters (M = orange and X = yellow) with equidistant spacings in the sodalite structure.

connected through two adjacent cage "double 6-ring" faces, whereas in zeolite A the sodalite units are hooked together with adjacent cage "double 4-ring" faces. The consequence of this is that in zeolite Y the eight-atom cluster corners are directed towards each other with a closest cluster-cluster contact distance of 4.4 Å based on van der Waals radii (Fig. 4C). The corresponding cluster contact distance in zeolite A is 7.6 Å (Fig. 9A) with a corresponding blue shift of the CdS absorption band edge from 370 to 320 nm.

Another way in which the sodalite cage units can be assembled is shown in Fig. 9B. In this case, the cages are packed sharing faces in an all space filling, cubic framework (a Federov solid) to give the closest possible approach between the cage contents. The framework composition and charge of the sodalite β cage in this structure can be varied as shown in Table 1 to give compositions such as $(B_2O_4)_3{\cdot}Zn_4S$ (*63*), $(B_2O_4)_3{\cdot}Zn_3GaP$, and $(BeSiO_4){\cdot}Cd_4Se$ (*64*). In the sodalite-type structures, the cage has the same acentric point group symmetry as ZnS or GaP, that is, $\bar{4}3m$, and contains, for example, the tetrahedral Zn_4S fragment, which is the first coordination sphere of the S atom in the bulk ZnS structure.

One therefore has an expanded semiconductor superlattice of Zn_4S molecular clusters. If one uses a larger anion X at the center of the sodalite cage, the Zn atoms are forced more toward the ultimate limit of being positioned at the center of the 6-ring openings. At that point the system becomes an expanded semiconductor lattice with all Zn atoms equally spaced from all X atoms at the centers of the cages (Fig. 9C). In the real structure of $(B_2O_4)_3{\cdot}Zn_4S$, a 1.1 Å displacement of the Zn atoms is required to remove the Zn_4S cluster identity.

The shift in the absorption edge as one proceeds from the furthest separated (~5.0 Å) sodalite cages in zeolites Y (Zn_4S_4) and Y (Cd_4S_4) to the closest packed sodalite configurations with (Cd_4S) and (Zn_4S) is shown in Fig. 10 (*65*). The optical absorption spectra of these systems for the boralite, berylsilicate, and berylgermanate frameworks are characterized by extremely sharp absorption edges that are typically blue-shifted from the bulk edge by 20 to 40 nm. The emission spectra at room temperature are intense and well defined with corresponding excitation spectra that show considerable structure and have a sharp excitation peak at the absorption edge. In the case of $(BeSiO_4)_3{\cdot}Cd_4S$ an emission exciton peak is also observed at the band edge.

Studies by Ozin and co-workers on the sodalite family $(AlSiO_4)_3{\cdot}Na_{4-n}Ag_nX$ have shown that these materials exhibit a variety of qualitative optical responses including baro-, hydro-, photo-, and thermochromism. Reversible read-write cycles (~70) with thermal erasure were also carried out (*44, 66*).

The quantum-confined Ag_nX (X = group VII atom) clusters that make up the superlattice show remarkable structural and spectroscopic transformations as one varies the sodalite cage occupancy

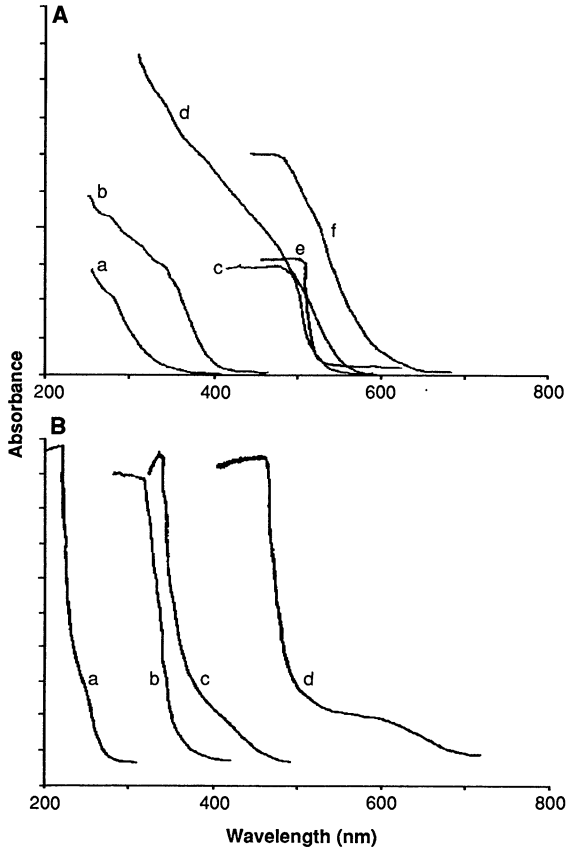

Fig. 10. (**A**) Comparison of the adsorption spectra of CdS in several hosts and with the bulk material: (a) CdS in zeolite Y, low loading; (b) CdS in zeolite Y, high loading; (c) CdS in helvite; (d) 1-μm CdS particles; (e) CdS in boralite; and (f) bulk CdS. (**B**) Comparison of the adsorption spectra of ZnS in several hosts and with bulk materials: (a) ZnS in zeolite Y; (b) ZnS in boralite; (c) bulk ZnS; and (d) bulk ZnSe.

(*45*). At very low loadings the AgX is a molecular silver halide unit with a Ag-X internuclear distance (2.21 Å for AgBr in the $Na_{3.7}$-$Ag_{0.3}$ cluster) that is shorter than that reported for gas-phase silver halide (2.39 Å). Because of the more extensive covalent bonding of AgBr compared with NaBr, the Na_3AgBr aggregate behaves like a slightly perturbed AgBr molecule with nearby Na^+ ions. In the fully exchanged Ag_4Br sodalites, the Ag-X (X = Cl, Br, or I) distances are ~8% shorter than in the rock salt bulk materials. The intercage Ag-Ag distances are 25 to 12% longer (Cl^- to I^-) than in the bulk structure.

The optical absorption data confirms the increased tunneling efficiency and intercage coupling as the distances between centers of the β cages decrease in the I^- to Cl^- sequence. At very low cluster loadings the transitions are similar to the gas-phase values of 230 and 320 nm for the AgBr monomer. Another interesting feature is evidence of a percolation threshold as seen in an abrupt change in the unit cell parameters and FT–far IR cation translatory modes as the silver-ion cage concentration increases.

In summary, in sodalite-type systems site occupancies, interatomic distances and overall crystallinity can be determined very precisely. Cage dimensions can be fine-tuned by using different framework atoms, and the cage occupancy can be easily varied. Mixed semiconductor lattices without cluster disorder are also possible. The sodalite class of materials present the best possibilities for growing large single crystals, and near optically useful sizes (3 mm) are already available. Most importantly, the quality of the quantum superlattice for this family is excellent and further studies can be expected to lead to a much clearer understanding of potential barriers and tunneling in 3-D quantum-confined superlattices.

Conclusions

The use of the 3-D crystalline superlattice as a host adds several important dimensions to the design of semiconductor quantum-confined structures. Cluster geometry and size distribution are controlled by the topography of the 3-D host surface, making it possible to create semiconductor quantum superlattices. Novel, normally very unstable, nanosized clusters can be synthesized by stabilization through encapsulation and coordination to the host framework. The use of large 3-D surface areas permits concentration studies of cluster interactions over a wide range and at relatively high optical densities. Cluster electronic properties can be altered by varying the dielectric and charge properties of the nanoporous host.

For optical studies, larger single crystals or thin films are needed. This shortcoming is being addressed by several groups as noted in the earlier discussion; and, the possible novel photonic or electronic properties of molecular sieve nanocomposites (*67*) is resulting in a new approach to molecular sieve synthesis. Much of the past research in the synthesis of such hosts has been in conjunction with their use as high-temperature catalysts so that the exploratory chemistry was limited by that goal. Low-temperature routes to new open framework materials that no longer contain only tetrahedral connecting atoms are rapidly becoming available. Some of these, such as the recently reported molybdenum(V) phosphates of Haushalter (*68*), contain five or six coordinate framework atoms (Mo^{5+}) and have host structures built up of $Mo_4O_8^{4+}$ cubes. In addition, Flanigen and co-workers have recently shown that substitution of S for O atoms in open-framework materials is possible; this discovery changes the insulating nature of the framework and is yielding many new structure types (*69*). These developments and the ability to generate zeolite membranes (*31*) mean that the sometimes tedious but necessary process of developing the art of growing optical quality centimeter-size molecular sieve crystals or preparing optical quality films is around the corner. It also suggests that some intriguing combinations of host and guest might be used.

One final note about the use of host/guest chemistry to obtain both structural information about the clusters and intercluster interactions and the ability to measure linear and nonlinear optical properties follows. We have thus far described materials that more or less fall into two categories, those where the size and interaction of particles are controlled by inclusion in crystalline hosts and those derived from arrested precipitation approaches where the intercluster interactions are not defined, but because they are in solution their optical properties are easily measured. If there were some way of using the complimentary information from these two approaches, one might be able to correlate the structural features, that is, cluster size, shape, and intercluster interactions, to observed optical properties. This would greatly facilitate the definition of parameters for improving both the optoelectronic responses and the very subtle chemistry necessary to build up extended bulk solids from molecular clusters.

One possible avenue is to take what is known about the chemistry of the inclusion of semiconductors in crystalline hosts and do the same chemistry in amorphous hosts, that is, porous glasses. Porous glasses, of course, can have optical transparency for critical measurements, but also they can be chemically similar to molecular sieves in that they have a pore structure (although random) and they can be based on similar framework compositions. The combination of molecular sieve quantum confinement and porous glass chemistry could lead to the development of practical NLO devices. With further study of both systems (crystalline and glass), one can expect new levels of understanding and applications of this fascinating regime of the solid state.

REFERENCES AND NOTES

1. D. Z. Anderson, *MRS Bull.* **13**, 30 (1988); for a recent review of these applications, see A. M. Glass, Ed., "Photonic Materials", *ibid.*, no. 8.
2. An excellent example is the recent announcement by IBM Yorktown Heights of the development of experimental computer chips for transmitting and receiving data over fiber optic lines at speeds of one billion bits per second. Each chip has more than 8000 transistors with characteristic features as small as 1 μm. One "receiver" chip holds 50 times more optical and electronic components than ever previously assembled on a chip for optoelectronic data transmission. Quantum-well confinement technology is used to create the light pulses for data transmission [*MRS Bull.* **14**, 12, (1989)].
3. S. Schmitt-Rink, D. A. B. Miller, D. S. Chemla, *Phys. Rev. B.* **35**, 8113 (1987); S. Schmitt-Rink, D. S. Chemla, D. A. B. Miller, *Adv. Phys.* **38**, 89 (1989).
4. Y. Wang, N. Herron, W. Mahler, A. Suna, *J. Opt. Soc. Am. B* **6**, 808 (1989).
5. N. Herron, paper presented at the Fifth Annual International Symposium on Inclusion Phenomena and Molecular Recognition, Perdido Beach, FL, September 1988.
6. C.-Y. Liu and A. J. Bard, *J. Phys. Chem.* **93**, 3232 (1989); *ibid.*, p. 7749.
7. R. P. Messmer and G. D. Watkins, *Phys. Rev. Lett.* **25**, 656 (1970); R. P. Messmer, *Phys. Rev. B* **15**, 1811 (1977); L. Esaki and R. Tsu, *IBM J. Res. Div.* **14**, 61 (1970); R. Tsu and L. Esaki, *Appl. Phys. Lett.* **22**, 562 (1973); R. Dingel, W. Wiegmann, C. H. Henry, *Phys. Rev. Lett.* **33**, 827 (1974).
8. L. E. Brus, *J. Phys. Chem.* **90**, 2555 (1986); *IEEE J. Quantum Electron* **22**, 1909 (1987); A. Henglein, *Top. Curr. Chem.* **143**, 113 (1988); L. Sakaki, *Jpn. J. Appl. Phys.* **19**, L735 (1980).
9. D. S. Chemla, *J. Lumin.* **30**, 502 (1985); ——— and D. A. B. Miller, *J. Opt. Soc. Am.* **B2**, 1155 (1985).
10. W. H. Knox *et al.*, *Phys. Rev. Lett.* **54**, 1306 (1985); W. H. Knox *et al.*, *ibid.* **56**, 1191 (1986); S. Schmitt-Rink, D. S. Chemla, D. A. B. Miller, *Phys. Rev. B* **32**, 6601 (1985).
11. E. S. Smotkin *et al.*, *Chem. Phys. Lett.* **152**, 265 (1988).
12. M. L. Steigerwald and L. E. Brus, *Annu. Rev. Mater. Sci.* **19**, 471 (1989).
13. I. G. Dance, A. Choy, M. L. Scudder, *J. Am. Chem. Soc.* **106**, 6285 (1984).
14. R. M. Herath Banda, I. G. Dance, T. D. Bailey, D. C. Craig, M. L. Scudder, *Inorg. Chem.* **28**, 1862 (1989).
15. M. L. Steigerwald *et al.*, *J. Am. Chem. Soc.* **110**, 3046 (1988).
16. J. G. Brennan *et al.*, *ibid.* **111**, 4141 (1989).
17. C. T. Dameron *et al.*, *Nature* **338**, 596 (1989).
18. Y. Horikoshi, M. Kawashima, H. Yamaguchi, *Jpn. J. Appl. Phys.* **25**, L868 (1986).
19. R. D. Dupuis, R. C. Miller, P. M. Petroff, *J. Cryst. Growth* **68**, 398 (1984); R. C.

Miller, A. C. Gossard, D. A. Kleinman, O. Munteanu, *Phys. Rev. B* **29**, 7085 (1984).
20. P. M. Petroff, A. C. Gossard, R. A. Logan, W. Wiegmann, *Appl. Phys. Lett.* **41**, 635 (1982); J. Cibert *et al.*, *ibid.* **49**, 1275 (1986).
21. M. A. McCord and R. F. W. Pease, *J. Vac. Sci. Technol.* **B5**, 430 (1987).
22. A. P. Alivisatos, A. L. Harris, N. J. Levinos, M. L. Steigerwald, L. E. Brus, *J. Chem. Phys.* **89**, 4001 (1988).
23. D. Ricard, *Physica A* **157**, 301 (1989).
24. Y. Wang and W. Mahler, *Opt. Commun.* **61**, 233 (1987).
25. P. D. Persans, A Tu, Y.-J. Wu, M. Lewis, *J. Opt. Soc. Am. B.* **6**, 818 (1989).
26. N. Herron, G. D. Stucky, C. A. Tolman, *J. Chem. Soc. Chem. Commun.* **1986**, 1521 (1986).
27. N. Herron, *Inorg. Chem.* **25**, 4714 (1986).
28. For good general references on zeolite Y and molecular sieves in general, see D. W. Breck, *Zeolite Molecular Sieves* (Krieger, Malabar, FL, 1984); R. M. Barrer, *Zeolites and Clay Minerals as Sorbents and Molecular Sieves* (Academic Press, New York, 1978).
29. J. M. Bennett *et al.*, *ACS Symp. Ser.* **218**, 109 (1983).
30. T. C. Sollner, P. E. Tannenwald, D. D. Peck, W. D. Goodhue, *Appl. Phys. Lett.* **45**, 1319 (1984); D. F. Nelson, R. C. Miller, D. A. Kleinman, A. C. Gossard, *Phys. Rev. B* **34**, 8671 (1986); B. F. Levine, K. K. Choi, C. G. Bethea, J. Walker, R. J. Malik, *Appl. Phys. Lett.* **51**, 934 (1987); L. C. West and S. J. Eglash, *ibid.* **46**, 1156 (1985).
31. T. Bein, K. Brown, G. C. Frye, C. J. Brinker, *J. Am. Chem. Soc.* **111**, 7640 (1989); T. Bein, K. Brown, P. Enzel, C. J. Brinker, *Mater. Res. Soc. Symp. Proc.* **121**, 761 (1988).
32. V. N. Bogomolov, E. L. Lutsenko, V. P. Petranovskii, S. V. Kholodkevich, *Pis'ma Zh. Eksp. Teor. Fiz.* **23**, 528 (1976).
33. V. N. Bogomolov, *Fiz. Tverd. Tela. (Leningrad)* **15**, 1312 (1973).
34. P. Cherin and P. Unger, *Inorg. Chem.* **6**, 1589 (1967).
35. ———, *Acta Crystallogr. B* **B28**, 313 (1972); R. D. Burbank, *ibid.* **5**, 236 (1952); R. E. Marsh, L. Pauling, J. D. McCullough, *ibid.* **6**, 71 (1953); O. Foss and V. Janicks, *J. Chem. Soc. Dalton Trans.* **624**, (1980); Y. Miyamoto, *Jpn. J. Appl. Phys.* **19**, 1813 (1980); T. Takahashi, S. Yagi, T. Sagawa, K. Nagata, Y. Miyamoto, *J. Phys. Soc. Jpn.* **54**, 1018 (1985).
36. J. B. Parise *et al.*, *Inorg. Chem.* **27**, 221 (1988).
37. V. N. Bogomolov, V. V. Poborchii, S. V. Kholodkevich, *Pis'ma Zh. Eksp. Teor. Fiz.* **31**, 464 (1980).
38. V. N. Bogomolov, A. I. Zadorozhnii, V. P. Petranovskii, A. V. Fokin, S. V. Kholodkevich, *ibid.* **29**, 411 (1979).
39. K. Takmura, S. Hosokawa, H. Endo, S. Yamasaki, H. Oyangi, *J. Phys. Soc. Jpn.* **55**, 528 (1986).
40. Y. Katayama, M. Yao, Y. Ajiro, M. Inui, H. Endo, *ibid.* **58**, 1811 (1989).
41. Computer graphics were carried out with CHEMX from Chemical Design, Ltd., Oxford, U.K.
42. The nomenclature "4-ring," "6-ring," and so forth describes the number of tetrahedral atoms that make up the ring. Oxygen atoms bridge between the metal atoms so that the actual numbers of atoms defining the 4- and 6-rings are 8 and 12, respectively. The 18-ring channels contain 36 atoms around a central channel.
43. M. E. Davis, C. Saldarriaga, C. Montes, J. Garces, C. Crowder, *Nature* **331**, 698 (1988); *Zeolites* **8**, 362 (1988).
44. G. A. Ozin, A. Stein, J. P. Godber, G. D. Stucky, *J. Inclusion Chem.*, in press.
45. A. Stein, G. A. Ozin, G. D. Stucky, *J. Am. Chem. Soc.*, in press.
46. Y. Wang and N. Herron, *J. Phys. Chem.* **91**, 257 (1987).
47. N. Herron, Y. Wang, M. Eddy, G. D. Stucky, D. Cox, *Off. Nav. Res. Rep. TR-4* [order no. AD-A199402; available as National Technical Information Service (NTIS) abstr. no. 905,972 (1988)]; K. Moller, T. Bein, M. Eddy, G. Stucky, N. Herron, *Off. Nav. Res. Rep. TR-11* [order no. AD-A196090; available as NTIS abstr. no. 855,144 (1988)].
48. Y. Wang and N. Herron, *J. Phys. Chem.* **92**, 4988 (1988).
49. N. Herron *et al.*, *J. Am. Chem. Soc.* **111**, 530 (1989).
50. X. Liu and J. K. Thomas, *Langmuir* **5**, 58 (1989); K. Moller, M. M. Eddy, G. D. Stucky, N. Herron, T. Bein, *J. Am. Chem. Soc.* **111**, 2564 (1989).
51. J. E. Mac Dougall *et al.*, *J. Am. Chem. Soc.* **111**, 8006 (1989).
52. R. D. Stramel, T. Nakamura, J. K. Thomas, *J. Chem. Soc. Faraday Trans.* **184**, 1287 (1988).
53. M. A. Fox and T. L. Pettit, *Langmuir* **5**, 1056 (1989).
54. W. J. Mortier, E. Dendooven, and J. B. Uyttehoeven [in *Proceedings of the Sixth International Zeolite Conference*, D. Olson and A. Bisio, Eds. (Butterworths, Guildford, 1984), pp. 49–54] demonstrate this point with Ca ion exchange in zeolite Y.
55. J. E. Mac Dougall and G. D. Stucky, unpublished results.
56. K. Moller, T. Bein, N. Herron, W. Mahler, Y. Wang, *Inorg. Chem.* **28**, 2914 (1989).
57. D. H. Olson, R. J. Mikovsky, G. F. Shipman, E. Dempsey, *J. Catal.* **24**, 161 (1972).
58. R. C. Burns, R. J. Gillespie, W. C. Luk, D. R. Slim, *Inorg. Chem.* **18**, 3086 (1979).
59. G. A. Ozin and S. Ozkar, unpublished results.
60. T. Bein, D. B. Chase, R. D. Farlee, G. D. Stucky, *Stud. Surf. Sci. Catal.* **28**, 311 (1986).
61. T. Bein, R. F. Carver, R. D. Farlee, G. D. Stucky, *J. Am. Chem. Soc.* **110**, 4546 (1988).
62. S. D. Cox, thesis, University of California, Santa Barbara (1989). The isotherms were determined by repeated exposure of a zeolite sample to increasing vapor pressures of $(CH_3)_2Zn$ or $(CH_3)_2Hg$. Reversibility was determined by repeating the procedure at decreasing vapor pressure and finally at full vacuum.
63. C. Fouassier, A. Levasseur, J. C. Joubert, J. Muller, P. Hagenmuller, *Z. Anorg. Allg. Chem.* **375**, 202 (1970).
64. J. E. Mac Dougall *et al.*, unpublished results.
65. J. E. Mac Dougall *et al.*, *MRS Symp. Ser.*, in press.
66. G. A. Ozin, J. P. Godber, A. Stein, U.S. Patent, filed August 1988; A. Stein, thesis, University of Toronto (1988).
67. G. Ozin, A. Stein, A. Kuperman, *Angew. Chem.* **101**, 373 (1989).
68. R. C. Haushalter and F. W. Lai, *Angew. Chem. Int. Ed. Engl.* **28**, 743 (1989); R. C. Haushalter, K. G. Strohmaier, F. W. Lai, *Science* **246**, 1289 (1989).
69. R. L. Bedard, S. T. Wilson, L. D. Vail, J. M. Bennet, E. M. Flanigen, *Stud. Surf. Sci. Catal.* **49**, 375 (1989).
70. We thank our collaborators: N. Herron, Y. Wang, K. Moller, T. Bein, H. Eckert, T. E. Gier, K. L. Moran, W. T. A. Harrison, and S. D. Cox for their contributions, V. Srdanov for helpful discussions, and M. Stucky for the photographic work. G.D.S. acknowledges the financial support from the Office of Naval Research, the National Science Foundation, and the Du Pont Company which has made this work possible.